Metallic Glass as a Mechanical Material for Microscanners

Yu-Ching Lin, Yao-Chuan Tsai,* Takahito Ono, Pan Liu, Masayoshi Esashi, Thomas Gessner, and Mingwei Chen*

Microelectromechanical system (MEMS) actuators essentially have movable silicon structures where the mechanical motion can be activated electronically. The microscanner is one of the most successfully commercialized MEMS devices which are widely used for collecting optical information, manipulating light, and displaying images. While silicon is abundant, it is also brittle and stiff and when microprocessed, defects are not uncommon. These defects result in weakness under torsional stress and this has been the key factor limiting the scanning performance of the microscanner. Here a metallic glass (MG)-based microscanner is reported with MG as the material for the moving torsion bars. The low elastic modulus, high fracture toughness, and high strength of MG offers, for the first time, an ultralarge rotating angle of 146° with power consumption lowered to the microwatt range, and a smaller driving force and better actuation performance, than conventional single crystal silicon and polycrystalline silicon. The high spatial resolution and large scanning field of the MG-based microscanner are demonstrated in the tomographic imaging of a human finger. This development of an MG-based MEMS possibly opens a new field of low-powered MEMS devices with extreme actuation and enhanced sensing.

1. Introduction

Micromirror-based scanners are typical optical microelectromechanical system (MEMS) devices which have been commercialized for use over a wide range of mechanical applications. They are standard technology in robots, endoscopes,[1,2] optical switches,[3] displays,[4] and barcode scanners[1] and are used in a variety of ranging imaging instruments.[5] The development of MEMS is key to developing more sophisticated wearable devices at a time when the market is well primed for their release. A large rotating angle, low power consumption, low driving voltage, and system miniaturization are the key performance measures which have been continuously improved to satisfy the requirements of new applications. Most studies have been focused on modifying the hinge design[2–4] and advancing actuation approaches[6,7] for Si-based microscanners. However, no significant progress has been made and this can largely be attributed to the limitations imposed by the material itself. Microfabricated single crystal silicon (SCS) and polycrystalline silicon (poly-Si) are brittle and fracture is dominated by the interior defects that form during the dry etching process.[8–10] Thus, the fracture strength of microprocessed silicon materials relies on theoretical probability and not a precise practical value and has obvious sample size dependence.[9] As such, the limitation of both single and poly crystalline microfabricated silicon materials renders them unsuitable for use as mechanical elements in long, thin structures subject to torsion. (Table S1, Supporting Information, shows comparison of mechanical properties between silicon materials and Zr-based metallic glass.) Crystal metals are common MEMS materials; however, they are not robust enough to provide long lifetime when constructed as a movable structure due to early mechanical fatigue. The mechanical properties of amorphous materials without crystalline defects are more predictable than the defect/flaw controlled mechanical properties of crystalline materials.[11] Amorphous metals exhibiting high strength and high elastic strain are promising MEMS materials and have been applied to certain devices and[12,13] a commercial device has successfully proofed the long life of small-angle-rotated mirrors by using amorphous metal as its hinge material.[14] However, residual stress in the deposited amorphous films remains an outstanding issue,[12] some electroplateable alloys had significant manufacturing deficiencies and low yields,[14] and the actuation performance of amorphous materials has not been investigated yet. Metallic glasses, unlike crystalline silicon and metal materials, they are strong and ductile, particularly on a small length scale,[15] furthermore the internal stress can be released by annealing in supercooled liquid region. These features make them valuable as mechanical elements in MEMS. Most applications of metallic glasses for MEMS are focused on

Prof. Y.-C. Lin, Dr. P. Liu, Prof. M. Esashi, Prof. M. Chen
WPI-Advanced Institute for Materials Research
Tohoku University
Sendai 980-8577, Japan
E-mail: yclin@mems.mech.tohoku.ac.jp
Dr. Y.-C. Tsai
MEMSCORE Cooperation
Sendai 981-3206, Japan
E-mail: yctsai@mems-core.com
Prof. T. Ono
Graduate School of Engineering
Tohoku University
Sendai 980-8579, Japan
Prof. T. Gessner
Fraunhofer ENAS and Chemnitz University of Technology
Chemnitz 09126, Germany

DOI: 10.1002/adfm.201502456

utilizing their formability in the supercooled liquid regions to form micro/nanoelements.[16–21] However, the batch fabrication is difficult using conventional molding techniques, and on-chip integration is also a major challenge. Thin film lift-off process of metallic glasses[21–23] has been used; however, thick film lift-off and deep dry etching approaches are still lacking. Here we develop standard MEMS compatible thick film lift-off as well as deep dry etching fabrication process of $Zr_{55}Cu_{30}Al_{10}Ni_5$ metallic glass[24,25] and report the successful implementation of it as the movable elements in microscanners. An unprecedented microscanner with a large rotating angle, high reliability, low power consumption, and low driving voltage has been realized using metallic glass.

2. Experiments

2.1. Properties of Thin Film Metallic Glass

Glassy ZrCuAlNi alloy thin film was sputtered onto a silicon substrate under the sputtering conditions of 0.4 Pa Ar working pressure and 70 W working power. The interface between the thin ZrCuAlNi film and the silicon substrate was observed by high resolution transmission electron microscopy (HRTEM). In the image shown in **Figure 1**a, the insightful bonding interface of the two materials as well as the amorphous structure of the as-deposited ZrCuAlNi can be clearly identified. The thin film density was calculated by weight divided by volume. The lift-off process of ZrCuAlNi was employed to define a certain deposition area. The weight was determined by subtracting the bare substrate from the thin film patterned substrate and the volume was obtained by the deposition area multiplied by the film thickness. The density of the ZrCuAlNi thin film was measured to be 6432 kg m^{-3}. The Young's modulus was obtained by detecting the resonant frequencies of ZrCuAlNi film cantilever beams.[26] The natural frequencies of free cantilever beams without considering air damping is given by

$$f_i = \frac{\lambda_i^2 t}{4\pi}\left(\frac{E}{3\rho}\right)\left(\frac{1}{l^2}\right) \quad (1)$$

where E, ρ, l, and t are the Young's modulus, density, length, and thickness of the cantilever beam, while λ_i is the eigenvalue, where i is an integer that describes the resonance mode number. In this work, the Young's modulus is calculated using the first vibration mode with λ_1 of 1.875. The experimentally

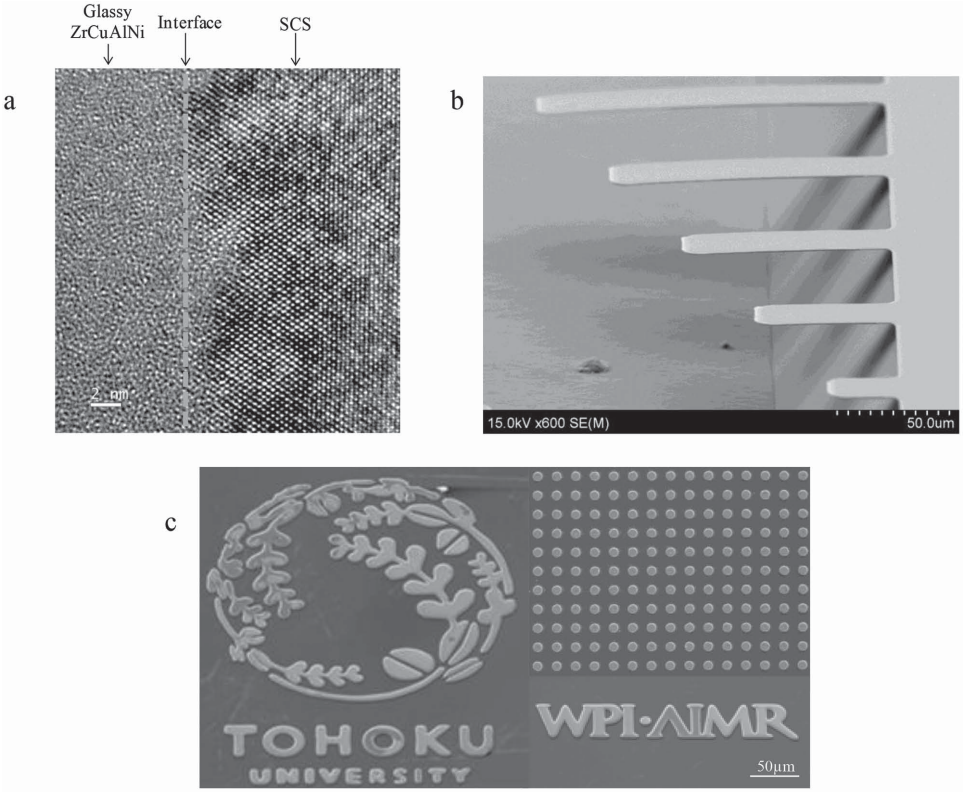

Figure 1. Electron microscope images of as-deposited and microstructured metallic glass ZrCuAlNi thin films. a) A HRTEM image of the as-deposited ZrCuAlNi alloy on a single crystal silicon substrate. ZrCuAlNi and silicon are bonded intimately at the atomic scale, indicating satisfied integration for further processing and application. The amorphous structure of ZrCuAlNi films is confirmed. b) ZrCuAlNi cantilever beams fabricated by lift-off and silicon wet etching process to determine the elastic coefficient. The cantilever beams range in length from 30 to 150 μm, with a width of 8 μm and a thickness of 1 μm. The resonant frequencies are obtained through laser-Doppler vibrometry and are subsequently employed to carry out the Young's modulus of ZrCuAlNi thin film to 95.05 GPa. c) Scanning electron microscope (SEM) images of 1 μm ZrCuAlNi thin films patterned by the RIE technique which removes the atoms by ion bombardment. 0.2 Pa Ar and 0.07 Pa C_4F_8 are mixed as the etching gases. The etching rate on the glassy thin films was 20 nm min^{-1}. The bright parts are the metallic glass.

measured resonant frequency was equal to the natural frequency. ZrCuAlNi cantilevers of various dimensions were fabricated by the lift-off technique[27] and silicon bulk etching process, as shown in Figure 1b. The Young's modulus of the thin film ZrCuAlNi was calculated at ≈95.05 GPa.

2.2. Microfabrication of Thin Film Metallic Glass

The MEMS fabrication compatibility of the ZrCuAlNi thin films was investigated by developing a dry etching process[28] and testing the chemical resistance. Figure 1c shows a 1 μm thick ZrCuAlNi pattern formed by reactive ion etching (RIE) batch process, in which a mixture of argon (Ar) and octafluorocyclobutane (C_4F_8) was used as an etching gas. Positive photoresist (AZ P4620, AZ Electronic Materials) was employed as the etching mask. Figure S1 (Supporting Information) shows the process steps. In the wet etching investigation, amorphous ZrCuAlNi was shown to have a high chemical resistance to the standard microfabricating wet process, such as potassium hydroxide, tetramethylammonium hydroxide, nitric acid (HNO_3), chromium etchant (mixtures of perchloric acid ($HClO_4$), and ceric ammonium nitrate ($(NH_4)_2[Ce(NO_3)_6]$) and gold etchant (mixtures of KI and I_2). However, it is not tolerant to hydrogen-fluoride-based chemicals or hydrochloric acid (HCl).

3. Results and Discussion

3.1. Metallic Glass Microscanner

A MEMS scanner made of a single crystal silicon substrate integrating metallic glass ZrCuAlNi as the material for the torsion bar was designed, developed, and microprocessed. **Figure 2**a shows the schematic of the metallic glass microscanner, consisting of a movable mirror plate fabricated from metallic glass and silicon. Under the metallic glass layer, a thick layer of silicon was structured to enhance the stiffness and thus avoid any deformation of the mirror surface during motion. The two torsion bars designed at each side of this micromirror

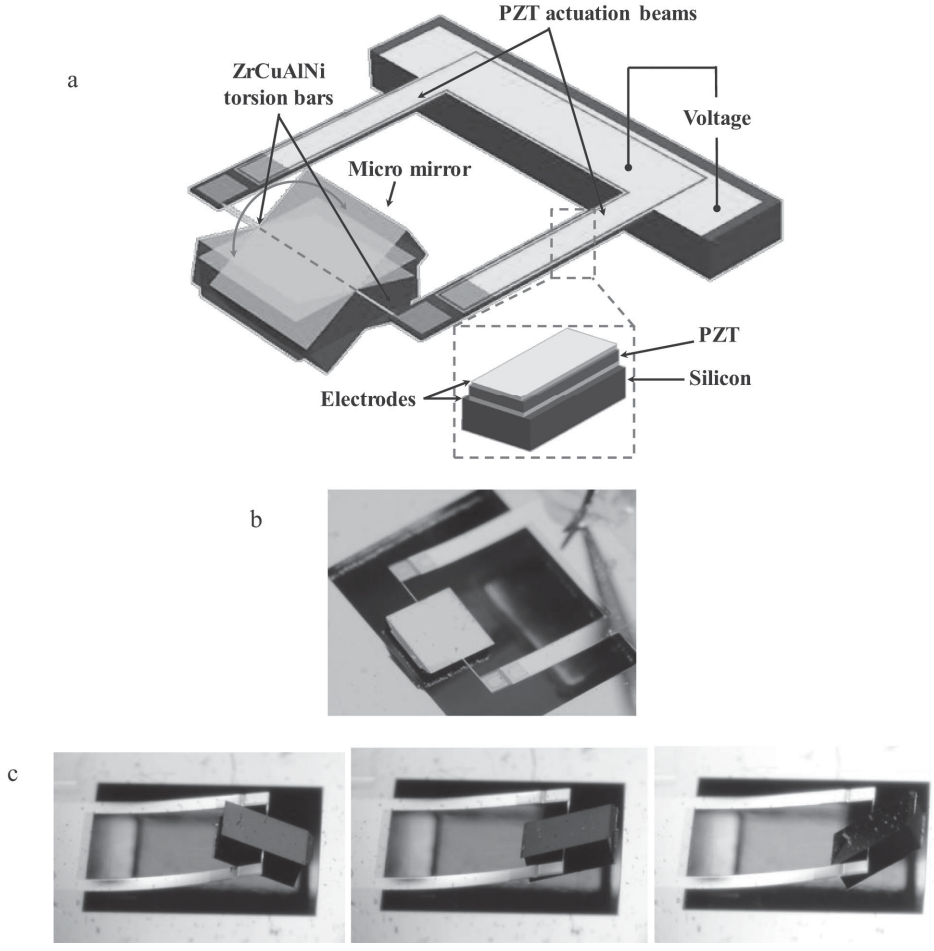

Figure 2. Piezoelectric-driven metallic glass microscanning mirror. a) Schematic illustration of the device design. Metallic glass ZrCuAlNi is employed as the tension bar material for mechanical motion. PZT actuation beams, consisting of a top electrode, a PZT layer, a bottom electrode, and a silicon supporting cantilever, are used to provide mechanical torque to the mirror plate. By applying AC voltage to the two side electrodes, the PZT layers bend up and down to generate actuation. b) The fabricated microscanner device. c) Metallic glass microscanner actuated by impressed voltage to PZT actuation beams. When the vibration frequency is equal to the torsion mode resonant frequency of the torsion bars, a large scanning angle is possible.

were fabricated only by thin films of metallic glass. The use of ZrCuAlNi thin film instead of the traditional silicon material marks a radical improvement in both toughness and actuation performance and a significant reduction in the driving voltage for the movable torsion bars. The torsion bars linked the micromirror to the two lead zirconate titanate (PZT) actuation beams used to excite rotational mirror motion. When AC voltage is applied to the electrodes of PZT, the actuation beams deform and introduce torque to the mirror plate, which results in a vibration of the micromirror. The 2 μm thick ZrCuAlNi film was patterned by lift-off and integrated into the standard silicon processes to fabricate the metallic glass micromirror. Figure S2 (Supporting Information) shows the process flow. The fabricated ZrCuAlNi micromirror consists of a 1000 μm square, 302 μm thick mirror plate, and one pair of 350 μm long, 10 μm wide, 2 μm thick metallic glass torsion bars (Figure 2b). The mirror was vibrated at its torsion mode resonant frequency of around 55.1 Hz (Figure 2c) to obtain a large tilting angle in an ambient atmosphere. Video in the supporting information exhibits the vibrating motion of the microscanner. The large rotation of the micromirror made possible by the metallic glass torsion bars allowed for considerable improvements in the scanning ability of the MEMS device. Since long thin structures made of silicon are known to be brittle under torsion,[9] we designed a long thin structure made of metallic glass to test its relative strength.

3.2. Performance of Metallic Glass Mechanical Component

The fabricated metallic glass microscanner uses microwatt level power consumption: a 146° rotating angle was achieved by 3.6 peak-to-peak driving voltage (V_{pp}). To the best of our knowledge, this is both the lowest power consumption and largest rotating angle ever achieved among all the reported torsion bar equipped MEMS scanners. Figure S3 (Supporting Information) shows the experimental setup of rotating angle measurements. **Figure 3**a shows the detected optical scanning angles under various driving voltages. The mirror plate tilts 0.7° even with 0.01 V_{pp} and attains a 146° rotation angle with a maximum 3.6 V_{pp} of actuation voltage. The realization of such a large rotating angle is possible due to the small elastic coefficient and the fine dimensions of the moving torsion bars fabricated by metallic glass. Equation (2) describes the relationship between the torsion angle and the construction conditions of rectangular-shaped torsion bars in the elastic region, in which T, w, h, and L are the applied torque, width, thickness, and length of the torsion bar

$$\theta = \frac{TL}{c_2 G w h^3} \tag{2}$$

The low spring constant of the tough metallic glass torsion bars allows them to be tilted through a thin dimension without failure. Clearly, the most critical factor for the large tilting angle is that very thin metallic glass torsion bars can be fabricated. It is extremely difficult to actuate crystalline silicon torsion bars on a long, thin structure due to their low fracture toughness and small shear loading tolerance, and it is especially challenging when the dimensions are so fine. With a low torsional modulus and their fine dimensions, the metallic glass mirror only requires a driving torque of 2.94×10^{-9} Nm to rotate at its maximum tilting angle of 146° in ambient. In case of operating the scanner in vacuum, the driving torque will be much smaller. The mechanical hysteresis of the metallic glass microscanner was investigated in the linear response region below a driving voltage of 3 V_{pp}. Almost no mechanical hysteresis can be seen when the rotating angle is smaller than 87.5°. Figure 3b shows the electric power consumption under various driving voltages calculated from the measured current consumption. When actuating a 6° scanning angle using 0.1 V_{pp}, 0.15 μA was applied and only 7.5 nW was consumed. When rotating at a 136° scanning angle using 3 V_{pp}, the applied current was 4.07 μA and the power consumption was 6.1 μW. Compared to commercially available MEMS scanners and the various MEMS scanners reported in the literature,[1,5] all of which require milli level watt power consumption, our metallic glass scanner requires only several nano to several microwatts, representing a dramatic drop to ultralow digit values.

Compared to SCS and poly-Si materials of the same dimension, the metallic glass torsion bars exhibit just 68% and 50%,

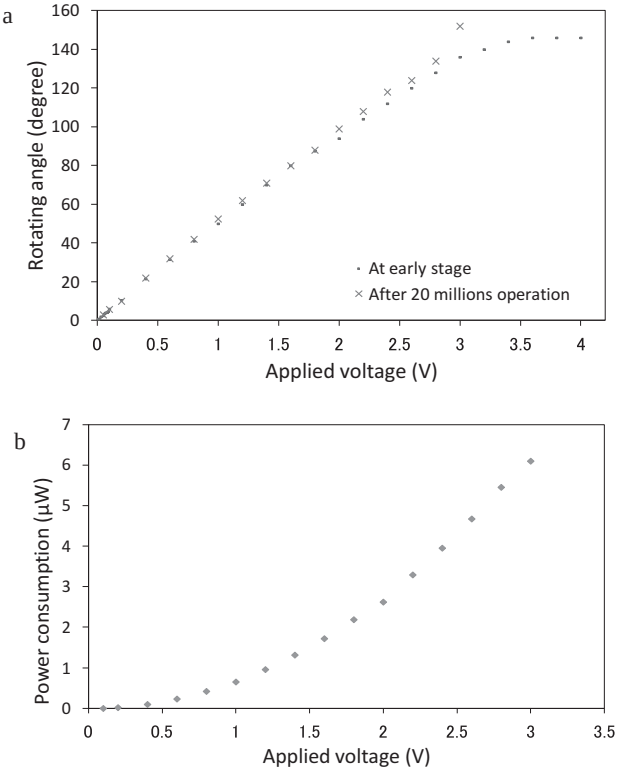

Figure 3. Rotating performance and power consumption of fabricated metallic glass microscanner. a) Large rotating angles of the mirror up to 146° are created by low applied voltage values up to 4 V. After 20 million cycle operations, almost no mechanical hysteresis appeared below a scanning angle of 87.5°. b) A dramatic decrease in power consumption to the nano/microwatt range was noted when using metallic glass torsion bars. Driving voltages above 1.4 V carry out a scanning angle of more than 70° with microlevel watt power consumption, driving voltages between 0.4 and 1.2 V allow for a 21.5°–60° scanning angle at the submicron watt level, while driving voltages below 0.2 V allow a scanning angle under 10.5° at the nanolevel watt level.

Table 1. Device performance of metallic glass microscanner in comparison with SCS and poly-Si microscanners of the same dimension.

Conditions	Compare to SCS	Compare to poly-Si
Mechanical loading stress at the same rotating angle	68%	50%
Breaking tilting angle (base on flexure stress coefficient)	17% large	32% large
Tilting performance at the same external driving torque	1.47 times	1.99 times
Power consumption at the same rotating angle	46%	25%

respectively, of the static internal loading stress, a 17% and 32% larger breaking tilting angle, 1.47 and 1.99 times better tilting performance, and a 46% and 25% decrease in power consumption, as shown in **Table 1**. Based on Equations (2) and (3), the mechanical loading from the maximum shear stress is defined as Equation (4)

$$\tau_{\max} = \frac{T}{c_1 w h^2} \tag{3}$$

$$\tau_{\max} = \theta G\left(\frac{c_2}{c_1}\right)\left(\frac{h}{L}\right) \tag{4}$$

The coefficients c_1 and c_2 are dependent on the ratio of the width to the thickness, and here $c_1 = c_2 = 0.291$.[29] For calculation purposes, the torsional modulus of ZrCuAlNi, SCS and poly-Si are assumed to be 34.7, 50.9, and 69 GPa, respectively. The breaking tilting angle is calculated from the flexure stress coefficient, defined as the yield stress divided by the torsional modulus.[30] While the results indicate that silicon torsion bars have the theoretical capability to be tilted to an ultralarge angle similar to that of ZrCuAlNi material, in actual situations their low fracture toughness and small shear loading tolerance prohibits this. On the other hand, the very large fracture toughness of metallic glass materials means metallic glass torsion bars can realize their theoretical performance without being compromised. Figure S4 (Supporting Information) shows the theoretical tilting performance and mechanical loading compared to SCS and poly-Si materials of the same dimension.

3.3. Application of Optical Coherence Tomography (OCT) Imaging

An OCT[31,32] image of a human finger was demonstrated by using the metallic glass-based microscanner connected to a commercial OCT system (HSL-2100-HW, Santec) to show one practical application. In the image in **Figure 4**, the cuticle, epidermis, dermis, and sweat grand can be clearly distinguished. The fingertip image with a lateral resolution of 4 µm was acquired by utilizing a metallic glass microscanner with 47 Hz resonant frequency, with a 28° scanning angle and 555 nW power consumption, by applying 1 V_{pp} and an object distance of 4 mm to the mirror device. The lateral resolution of the topographic image obtained was approximately an order of magnitude higher than the OCT images obtained using silicon torsion bar microscanners.[33–35] The lateral resolution is inversely proportional to the micromirror scanning frequency, indicating that a low resonant frequency leads to high resolution. By fabricating an ultimate torsion bar dimension and a thick mirror plate, the metallic glass microscanner can easily reach a low resonant frequency. Attaining such conditions when using silicon torsion bars is, however, extremely difficult. Using the metallic glass microscanner, it was possible to realize a host of firsts for MEMS scanner acquired OCT imaging: ultrahigh resolution, ultralow power consumption, an ultralarge scanning angle, and an ultrasmall driving voltage. What is even more remarkable is that they were achieved simultaneously. In addition, our investigation of the lifetime of the ZrCuAlNi mirror device by voltage impression to the PZT actuation beams revealed that more than 600 million cycle motions had

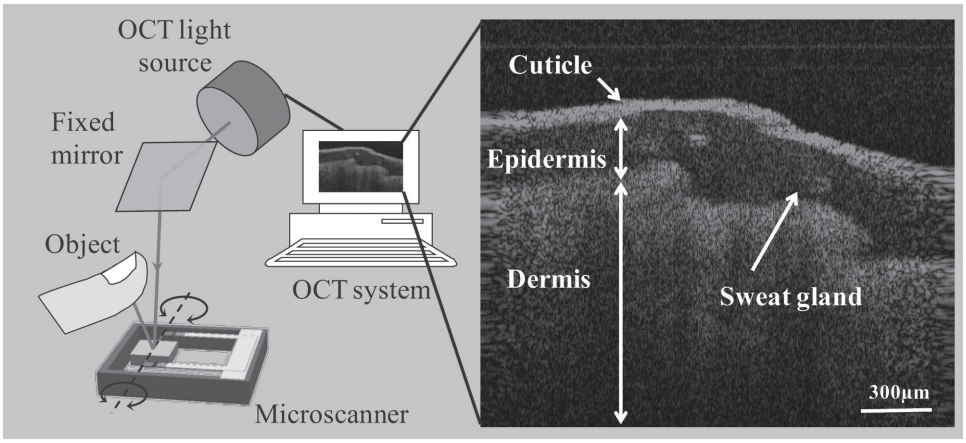

Figure 4. OCT bioimaging of fingertip obtained by a commercial OCT system with setting of the metallic glass microscanning mirror. Illustration of metallic glass microscanner set up for OCT demonstration and OCT imaging. The fingertip tomographic image with high lateral resolution is collected by the fabricated microscanner and transmitted to the commercial OCT system. The fine details, such as the sweat gland, cuticle, epidermis, and dermis, are clear.

been obtained without any indication of fatigue failure in the device, and the test is still ongoing.

4. Conclusion

Utilizing metallic glass as the movable structure material, the microscanner exhibits ultralow power consumption and ultrahigh rotating performance, which requires 7.5 nW and 6.1 μW for 6° and 136° scanning angles, respectively. Material characterization and MEMS compatible fabrication of thin film ZrCuAlNi were investigated and developed. Compare to conventional torsion bar materials of SCS and poly-Si on the same dimension, the metallic glass exhibits 68% and 50% static loading stress, 17% and 32% larger breaking tilting angle, 1.47 and 1.99 times tilting performances, and 46% and 25% power consumption. A high-resolution wide-scanning OCT bioimaging exhibits its practicability and the long lifetime reveals its reliability. The use of metallic glasses as a mechanical material for MEMS is expected to allow for development of ultralow power consumption devices and therefore vastly extend the operation period of batteries. Further research is expected to extend to the realization of a self-subsistence device accompanying the evolution of self-generation technology.[36] The development of these low-power-consumption high-performance metallic glass MEMS has high potential to meet the requirements of next-generation wearable and mobile technologies.

Supporting Information

Supporting Information is available from the Wiley Online Library or from the author.

Acknowledgements

Y.-C.L. and Y.-C.T. contributed equally to this work. This work was supported by the Regional Innovation Strategy Support Program (MEXT, Japan), the Tohoku University Exploratory Research Program for Young Scientists, the Creation of innovation centers for advanced interdisciplinary research areas Program (JST, Japan), and the WPI Advanced Institute for Materials Research of Tohoku University. The authors would like to acknowledge Takayuki Naono and Takamichi Fujii in Fujifilm Corporation for providing the PZT material and the assistance on taking the OCT images. Prof. Ioana Voiculescu is also appreciated for reading on the paper.

Received: June 16, 2015
Revised: July 13, 2015
Published online: August 10, 2015

[1] J. T. W. Yeow, V. X. D. Yang, A. Chahwan, M. L. Gordon, B. Qi, I. A. Vitkin, B. C. Wilson, A. A. Goldenberg, *Sens. Actuators, A* **2005**, *117*, 331.
[2] U. Hofmann, J. Janes, H.-J. Quenzer, *Micromachines* **2012**, *3*, 509.
[3] S. Schweizer, S. Calmes, M. Laudon, Ph. Renaud, *Sens. Actuators* **1999**, *76*, 470.
[4] T. Naono, T. Fujii, M. Esashi, S. Tanaka, *J. Micromech. Microeng.* **2014**, *24*, 015010.
[5] J. Yamaguchi, T. Sakata, N. Shimoyama, H. Ishii, F. Shimokawa, T. Yamamoto, *NTT Tech. Rev.* **2007**, *5*, 1.
[6] H. Schenk, P. Dürr, T. Haase, D. Kunze, U. Sobe, H. Lakner, H. Kück, *IEEE J. Sel. Top. Quantum Electron.* **2000**, *6*, 715.
[7] A. D. Yalcinkaya, H. Urey, D. Brown, T. Montague, R. Sprague, *J. Microelectromech. Syst.* **2006**, *15*, 786.
[8] T. Tsuchiya, M. Hirata, N. Chiba, R. Udo, Y. Yoshitomi, T. Ando, K. Sato, K. Takashima, Y. Higo, Y. Saotome, H. Ogawa, K. Ozaki, *J. Microelectromech. Syst.* **2005**, *14*, 1178.
[9] T. Ando, M. Shikada, K. Sato, *Sens. Actuators, A* **2001**, *93*, 70.
[10] X. Li, T. Kasai, S. Nakao, H. Tanaka, T. Ando, M. Shikida, K. Sato, *Sens. Actuators, A* **2005**, *119*, 229.
[11] D. C. Hofmann, J.-Y. Suh, A. Wiest, G. Duan, M.-L. Lind, M. D. Demetriou, W. L. Johnson, *Nature* **2008**, *451*, 1085.
[12] J. R. Porter, J. DeNatale, N. Gluck, D. Branagan, *Incorporation of Amorphous Metals into MEMS for High Performance and Reliability*, Report GO-71189, Report Rockwell Scientific Co., USA **2003**, p. 1.
[13] M. Ylönen, T. Vähä-Heikkilä, H. Kattelus, *Sens. Actuators, A* **2006**, *132*, 283.
[14] J. H. Tregilgas, *Adv. Mater. Process.* **2004**, *162*, 40.
[15] D. Jang, J. R. Greer, *Nat. Mater.* **2010**, *9*, 215.
[16] G. Kumar, H. X. Tang, J. Schroers, *Nature* **2009**, *457*, 868.
[17] G. Kumar, A. Desai, J. Schroers, *Adv. Mater.* **2011**, *23*, 461.
[18] M. Kanik, P. Bordeenithikasem, G. Kumar, E. Kinser, J. Schroers, *Appl. Phys. Lett.* **2014**, *105*, 131911.
[19] J. Schroers, Q. Pham, A. Desai, *J. Microelectromech. Syst.* **2007**, *16*, 240.
[20] M. Kanik, P. Bordeenithikasem, D. Kim, N. Selden, A. Desai, R. M'Closkey, J. Schroers, *J. Microelectromech. Syst.* **2015**, *24*, 19.
[21] H.-W. Jeong, S. Hata, A. Shimokohbe, *J. Microelectromech. Syst.* **2003**, *12*, 42.
[22] Y. Li, Q. Guo, J. A. Kalb, C. V. Thompson, *Science* **2008**, *322*, 1816.
[23] Y. Yokoyama, T. Fukushige, S. Hata, K. Masu, A. Shimokohbe, *Jpn. J. Appl. Phys.* **2003**, *42*, 2190.
[24] A. Inoue, T. Zhang, *Mater. Trans., JIM* **1995**, *36*, 1184.
[25] A. Inoue, Y. Kawamura, T. Shibata, K. Sasamori, *Mater. Trans., JIM* **1996**, *37*, 1337.
[26] L. Kiesewetter, J.-M. Zhang, D. Houdeau, A. Steckenborn, *Sens. Actuators, A* **1992**, *35*, 153.
[27] J.-W. Lee, Y.-C. Lin, N. Kaushik, P. Sharma, A. Makino, A. Inoue, M. Esashi, T. Gessner, *Opt. Lett.* **2011**, *36*, 3464.
[28] Y.-C. Tsai, Y.-C. Lin, T. Abe, M. Esashi, T. Gessner, *Proc. IEEE Sens.*, IEEE, Picastaway, NJ, USA **2012**, p. 339.
[29] W. C. Young, R. G. Budynas, *Roark's Formulas for Stress and Strain*, 7th ed., McGraw-Hill, New York **2002**.
[30] H. Urey, *Proc. SPIE* **2002**, *4773*, 27.
[31] D. Huang, E. A. Swanson, C. P. Lin, J. S. Schuman, W. G. Stinson, W. Chang, M. R. Hee, T. Flotte, K. Gregory, C. A. Puliafito, J. G. Fujimoto, *Science* **1991**, *254*, 1178.
[32] G. J. Tearney, M. E. Brezinski, B. E. Bouma, S. A. Boppart, C. Pitris, J. F. Southern, J. G. Fujimoto, *Science* **1997**, *276*, 2037.
[33] M. Nakada, C. Chong, A. Morosawa, K. Isamoto, T. Suzuki, H. Fujita, H. Toshiyoshi, *IEE J. Trans. Electr. Electron. Eng.* **2014**, *9*, 448.
[34] K. H. Kim, B. H. Park, G. N. Maguluri, T. W. Lee, F. J. Rogomentich, M. G. Bancu, B. E. Bouma, J. F. Boer, J. J. Bernstein, *Opt. Express* **2007**, *15*, 18130.
[35] A. D. Aguirre, P. R. Herz, Y. Chen, J. G. Fujimoto, W. Piyawattanametha, L. Fan, M. C. Wu, *Opt. Express* **2007**, *15*, 2445.
[36] Z. L. Wang, J. Song, *Science* **2006**, *312*, 242.